A Step Up Dc – Dc Converter With High Voltage Gain for Microsource Applications

Dinesh Kumar Munigala[#1] , J.Srinivas Rao[#2]

[#] *EEE Dept. Anurag Engineering College, JNTU- HYD*
Ananthagiri(vilg), Kodad, Andhrapradesh, India

dinesh.munigala@gmail.com

srinivasrao.eee@anurag.ac.in

***Abstract*— This paper proposes a new high step-up dc–dc converter designed especially for regulating the dc interface between various microsources and a dc–ac inverter to electricity grid. The converter achieves high step-up voltage gain with appropriate duty ratio and low voltage stress on the power switch. Additionally, the energy stored in the leakage inductor of the coupled inductor can be recycled to the output capacitor. The operating principles and steady-state analyses of continuous-conduction mode, discontinuous-conduction mode and boundary-conduction mode are discussed in detail. To verify the performance of the proposed converter, a simulation modelled converter is implemented with an input voltage range of 38 - 40 V and an output voltage of up to 380 - 400 V. The upmost efficiency of 95.3% is reached with high-line input; on the other hand, the full-load efficiency remains at 93% during low-line input.**

***Keywords*— Coupled inductor, Dc-Dc converter, high voltage gain, duty cycle, microsources.**

I. INTRODUCTION

RENEWABLE energy is becoming increasingly important and prevalent in distribution systems, which provide different choices to electricity consumers whether they receive power from the main electricity source or in forming a microsource not only to fulfill their own demand but alternatively to be a power producer supplying a microgrid. A microgrid usually includes various microsources and loads, which operate as an independent and controllable system when they are either grid-connected or islanded, as well as when they can reliably connect or disconnect. The microsource is classified either as a dc source or as a highfrequency ac source. These two microsource categories are comprised of diverse renewable energy applications, such as solar cell modules, fuel cell stacks, wind turbines, and reciprocating engines. Fig. 1.1 shows a regular schematic of a microgrid unit supplied by various microsources; the high step-up converter is used to increase the output voltage of the microsources from 40 V to 360–400 V for the dc interface to the main electricity source through the dc–ac inverter. Both the single solar cell module and the fuel cell stack are essentially low-voltage sources, and thus, a high step-up voltage gain dc–dc converter is required to regulate the voltage of the dc–dc interface.

The power capacity range of a microsources is about 100W to 500W, and the maximum power point (MPP) voltage range is from 15V to 40V, which will be the input voltage of the ac module; in cases with lower input voltage, it is difficult for the ac module to reach high efficiency. However, employing a high step-up dc–dc converter in the front of the inverter improves power-conversion efficiency and provides a stable dc link to the inverter.

The micro inverter includes dc–dc boost converter, dc–ac inverter. The dc–dc converter requires large step-up conversion from the microsource low voltage to the voltage level of the application. The converters by increasing turns ratio of coupled inductor obtain higher voltage gain than conventional boost converter. Some converters successfully combined boost and fly back converters, since various converter combinations are developed to carry out high step-up voltage gain by using the coupled-inductor techniques. By combining active snubber, auxiliary resonant circuit, synchronous rectifiers, or switched- capacitor-based resonant circuits and so on, these techniques made active switch into zero voltage switching (ZVS) or zero current switching (ZCS) operation and improved converter efficiency.

The proposed converter, shown in Fig. 1.2, is comprised of a coupled inductor $T1$ with the floating active switch $S1$. The primary winding $N1$ of a coupled inductor $T1$ is similar to the input inductor of the conventional boost converter, and capacitor $C1$ and diode $D1$ receive leakage inductor energy from $N1$. The secondary winding $N2$ of coupled inductor $T1$ is connected with another pair of capacitors $C2$ and diode $D2$, which are in series with $N1$ in order to further enlarge the boost voltage. The rectifier diode $D3$ connects to its output capacitor $C3$. The proposed converter has several features:1) The connection of the two pairs of inductors, capacitor, and diode gives a large step-up voltage-conversion ratio; 2) The leakage-inductor energy of the coupled inductor can be recycled, thus increasing the efficiency and restraining the voltage stress across the active switch.

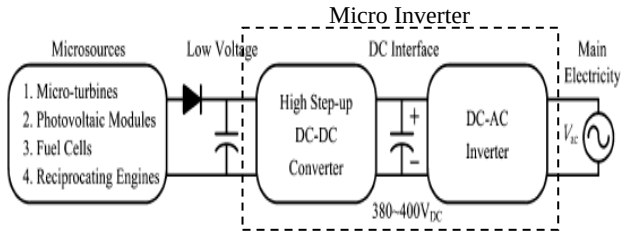

Fig 1. 1. Basic schematic of the microgrid consisted of diversely microsources and power converters.

The operating principles, steady-state analysis and duty ratio of the proposed converter are presented in the following sections.

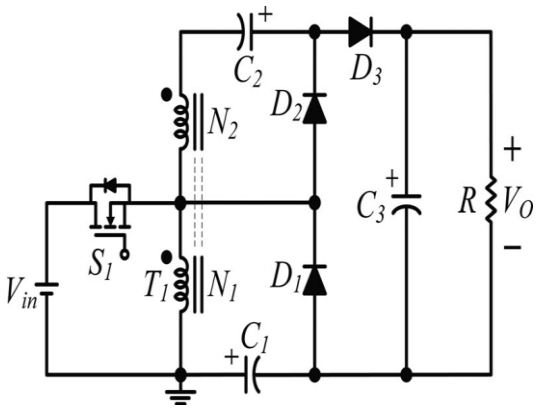

Fig 1.2 Circuit configuration of proposed converter.

II. Operating Principles of the Proposed Converter

The operation of the proposed converter is shown in Fig 2.1. The circuit is compressed with the coupled inductor T_1, T_1 is represented as a magnetizing inductor Lm, primary and secondary leakage inductors L_{k1} and L_{k2}, and an ideal transformer. In order to simplify the circuit analysis of the proposed converter, the following assumptions are made.

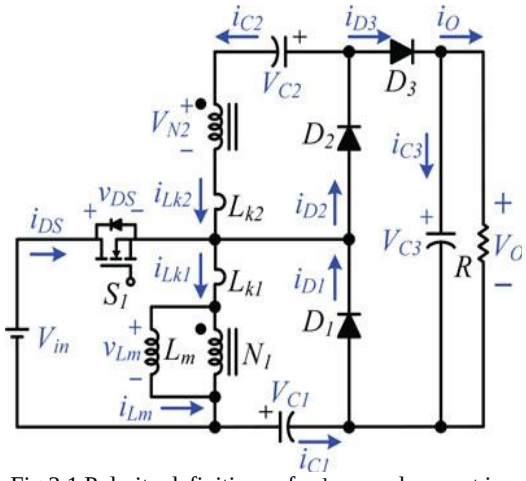

Fig 2.1 Polarity definitions of voltage and current in proposed converter.

1) All components are ideal, except for the leakage inductance of coupled inductor T1, which is being taken under consideration. The on-state resistance R_{DS} (ON) and all parasitic capacitances of the main switch S1 are neglected, as are the forward voltage drops of diodes D1 and D3.
2) The capacitors C1 and C3 are sufficiently large that the voltages across them are considered to be constant.
3) The ESR of capacitorsC1 and C3 and the parasitic resistance of coupled inductor T1 are neglected.
4) The turn's ratio n of the coupled inductor T1 windings is equal to N2 /N1.

The operating principle of continuous conduction mode (CCM) is presented in detail. The current waveforms of major components are given in Fig. 2.2. There are five operating modes in a switching period.

A. CCM Operation.

Mode I *$[t_0 - t_1]$:* when the mode operation is started in between the time interval (t_0-t_1) the transition interval, the magnetizing inductor Lm continuously charges capacitor C_2 through T_1 when S_1 is turned ON. The current flow path is shown in Fig. 2.3(a) Current i_{Lm} is decreasing because source voltage V_{in} crosses magnetizing inductor Lm and primary leakage inductor L_{k1} magnetizing inductor L_m is still transferring its energy through coupled inductor T_1 to charge switched capacitor C_2, but the energy is decreasing the charging current i_{D2} and i_{C2} are decreasing. The secondary leakage inductor current i_{LK2} is declining as equal to i_{Lm} / n. Once the increasing i_{Lk1} equals decreasing i_{Lm} at $t = t_1$, this mode ends.

Mode II *$[t_1 - t_2]$:* During this interval, the condition of the magnetizing inductor L_m is changed from releasing energy to storing energy from V_{in}. As a result, the switched capacitors also changed their condition from charging, to discharging energy to output. The current flow path is shown in Fig. 2.3(b). During this interval the source energy V_{in} is series connected with N_2, C_1, and C_2 to charge output capacitor C_3 and load R; meanwhile magnetizing inductor Lm is also receiving energy from V_{in}. The current flow path where switch S_1 remains ON, and only diode D_3 is conducting. The i_{Lm}, i_{Lk1} , and i_{D3} are increasing because the V_{in} is crossing L_{k1} , L_m, and primary winding N_1 ; L_m and L_{k1} are storing energy from V_{in} ; meanwhile V_{in} is also serially connected with secondary winding N_2 of coupled inductor T_1 , capacitors C_1 , and C_2 , and then discharges their energy to capacitor C_3 and load R. The i_{in}, i_{D3} and discharging current $|i_{C1}|$ and $|i_{C2}|$ are increasing. This mode ends when switch S_1 is turned OFF at $t = t_2$.

Mode III *$[t_2 - t_3]$:* When the time period (T_S) is operating at the time of $t_2 - t_3$interval, during this transition interval the secondary leakage inductor L_{k2} keeps charging C_3 when switch S_1 is OFF. The current flow path is shown in Fig 2.3(c), where only diode D_1 and D_3 are conducting. The energy stored in leakage inductor L_{k1} flows through diode D_1 to charge

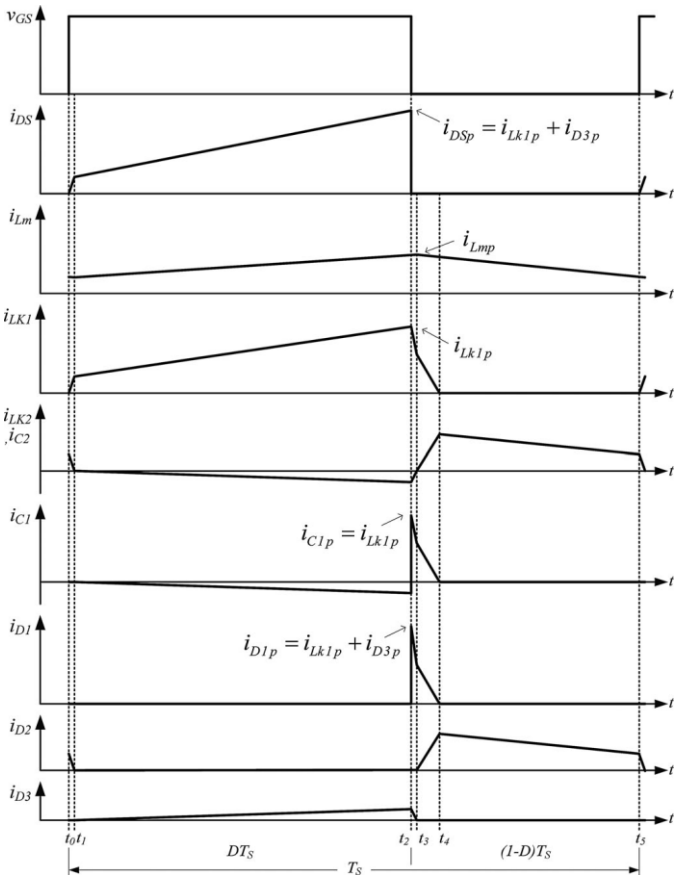

Fig 2.2 Typical waveforms of proposed converters at CCM operation

capacitor C_1 instantly when S_1 is OFF. Meanwhile, the energy of secondary leakage inductor L_{k2} is series connected with C_2 to charge output capacitor C_3 and the load. Because leakage inductance L_{k1} andL_{K2} are far smaller than Lm, i_{Lk2} rapidly decreases, but iLm is increasing because magnetizing inductor Lm is receiving energy from L_{k1}. Current i_{Lk2} decreases until it reaches zero; this mode ends at $t = t_3$.

Mode IV *$[t_3 – t_4]$:* When the time period is operating at the time of $t_3 – t_4$ interval, during this transition interval the energy stored in magnetizing inductor Lm is released to C_1 and C_2 simultaneously. The current flow path is shown in Fig 2.3(d) ; only diodes D_1 and D_2 are conducting. Currents i_{Lk1} and i_{D1} are continually decreased because the leakage energy still flowing through diodeD_1 keeps charging capacitor C_1. The Lm is delivering its energy through T_1 and D_2 to charge capacitor C_2. The energy stored in capacitor C_3 is constantly discharged to the load R. These energy transfers result in decreases in iLk1 and iLm but increases in i_{Lk2}. This mode ends when current i_{Lk1} is zero, at $t = t_4$.

Mode V *$[t_4 – t_5]$:* During this interval the only magnetizing inductor Lm is constantly releasing its energy to C_2. The current flow path which only diode D_2 is conducting. The iLm is decreasing due to the magnetizing inductor energy flowing through the coupled inductor T_1 to secondary winding N_2, and D_2 continues to charge capacitor C_2. The energy stored in capacitor C_3 is constantly discharged to the load R. This mode ends when switch S_1 is turned ON at the beginning of the next switching period.

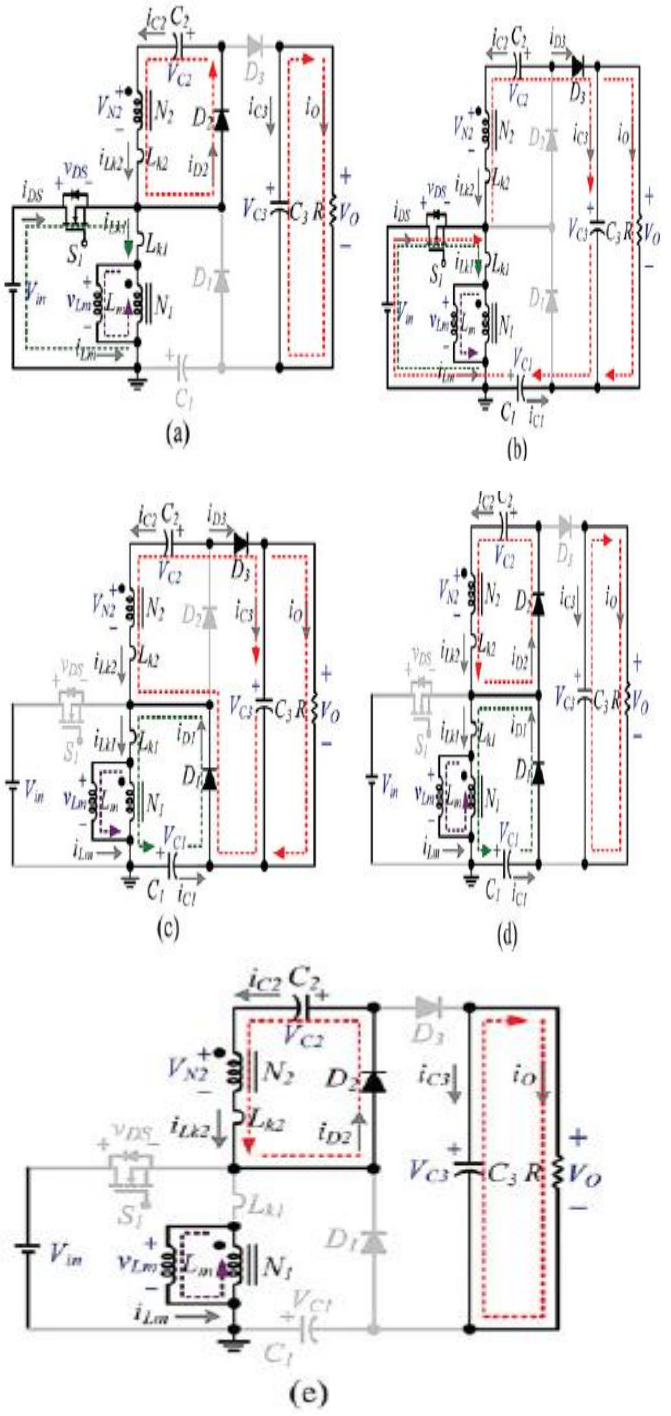

Fig 2.3: Current flow path in five operating modes during one switching period for CCM operation. (a)Mode I. (b) Mode II. (c) Mode III. (d)Mode IV. (e)Mode V.

III. DUTY CYCLE

In CCM, power transfer is a two-step process. When the switch is ON, stored energy builds in the inductor. When the switch is OFF, energy transfers to the output through the diode. The switch current is a stepped saw tooth with a fixed steady-state ON time with some amount of ripple current superimposed.

During the ON time of the switch, if we assume zero losses for the moment, the voltage across the inductor is approximately the input voltage; and the voltage across the rectifier is the capacitor, or output voltage. When the switch turns OFF, the energy stored in the inductor releases into the output through the rectifier. The voltage across the inductor is approximately the input-to-output voltage difference, and the voltage across the switch becomes approximately the output voltage Important to any model is the understanding of the current in each of the relevant components in the power path. The mathematical construction of these currents helps to determine the magnitude and shapes of these currents.

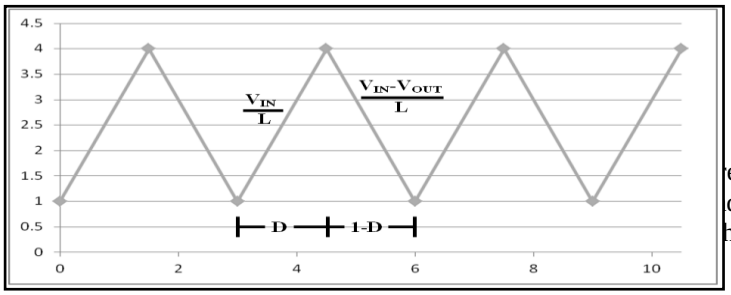

Fig 3.1: Current through Inductor

With zero losses assumed, the inductor current's ON-time slope is

$$m_{I_{L(ON)}} = \frac{V_{IN}}{L}. \quad \text{(i)}$$

During the OFF time, the current will have a slope of

$$m_{I_{L(OFF)}} = \frac{V_{IN} - V_{OUT}}{L}. \quad \text{(ii)}$$

Based on the slope of the rising and falling slopes of the current through the inductor and the fact that the time duration is a known entity, the transfer function can be computed.

$$\frac{V_{IN}}{L}(D) + \frac{V_{IN} - V_{OUT}}{L}(1 - D) = 0 \quad \text{(iii)}$$

Algebraic steps were used to isolate V_{OUT} which yields Equation.

$$V_{OUT} = \frac{V_{IN}D}{1 - D} + V_{IN} \quad \text{(iv)}$$

Solving for the switch duty cycle, D, results in

$$D_{CCM(ideal)} = 1 - \frac{V_{IN}}{V_{OUT}}. \quad \text{(v)}$$

The input losses include the inductor winding resistance (R_L), the switch MOSFET R_{DS} (ON), and (in the case of a current-mode-controlled converter) a current sense resistor (RISENSE). The output losses are represented by the output diode rectifier, D_1. If the loss elements of the power-stage components are included, the equation for the duty cycle in CCM is shown by Equation (v) above. Equation (v) holds true for CCM when the ripple current in the inductor is small relative to the average DC current. The equation is "close" when there is a high percentage of ripple current. Reassuringly, if the losses in Equation (v) reduce to zero, the equation simplifies to the ideal case.

IV. STEADY STATE ANALYSIS

To simplify the steady-state analysis, only modes II and IV e considered for CCM operation, and the leakage ductances on the secondary and primary sides are neglected. he following equations can be written from Fig.2.3:

$$v_{Lm} = V_{\text{in}} \quad (1)$$

$$v_{N2} = nV_{\text{in}}. \quad (2)$$

During mode IV

$$v_{Lm} = -V_{C1} \quad (3)$$

$$v_{N2} = -V_{C2}. \quad (4)$$

Applying a volt-second balance on the magnetizing inductor *Lm* yields

$$\int_0^{DT_S} (V_{\text{in}})dt + \int_{DT_S}^{T_S} (-V_{C1})dt = 0 \quad (5)$$

$$\int_0^{DT_S} (nV_{\text{in}})dt + \int_{DT_S}^{T_S} (-V_{C2})dt = 0 \quad (6)$$

From which the voltage across capacitors*C*1 and*C*2 are obtained as follows:

$$V_{C1} = \frac{D}{1-D} V_{\text{in}} \qquad (7)$$

$$V_{C2} = \frac{nD}{1-D} V_{\text{in}}. \qquad (8)$$

During mode II, the output voltage ***VO* = *Vin* + *VN* 2 + *VC* 2+ *VC* 1** becomes

$$V_{\text{O}} = V_{\text{in}} + nV_{\text{in}} + \frac{nD}{1-D} V_{\text{in}} + \frac{D}{1-D} V_{\text{in}}. \qquad (9)$$

The DC voltage gain MCCM can be found as follows:

$$M_{\text{CCM}} = \frac{\text{V}_{\text{O}}}{V_{\text{in}}} = \frac{1+n}{1-D}. \qquad (10)$$

V. Simulation Results

The Proposed Converter is designed and Simulated in MATLAB. The simulation results show that the maximum efficiency of the converter is about 93%.

The input voltage of the converter is given as 40 V and the output voltage obtained is 385 V with a Resistance load of 400Ω. The output power and the input power of the converter is calculated from simulated current and voltage waveforms and the maximum efficiency of the converter is found as 93%.

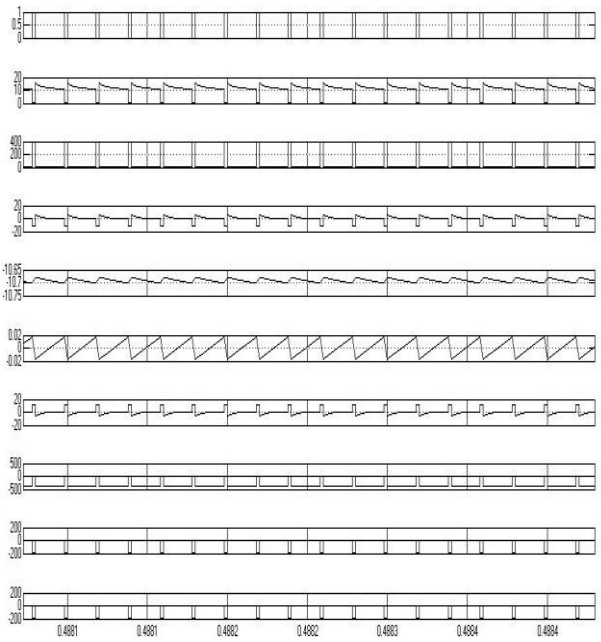

Fig: 5.1 Simulation results of Proposed Converter across various devices.

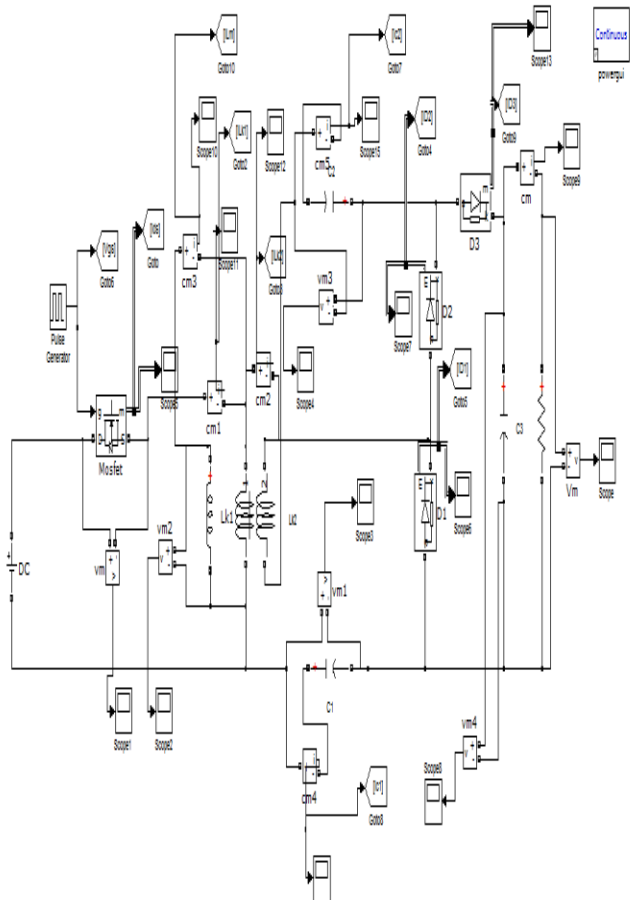

Fig: 5.2 Simulation Model of Proposed Converter

The proposed converter is simulated at different Resistance loads and calculated its efficiency is calculated at various load. The efficiency V/s R Load graph is shown below in fig. 5.3.The proposed Dc-Dc converter output voltage waveform is shown in Fig. 5.6.

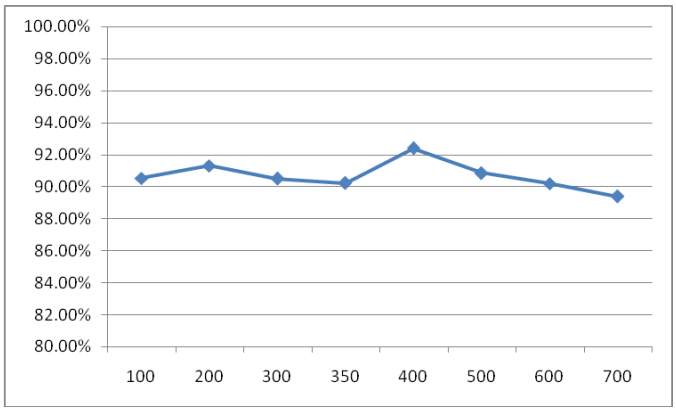

Fig: 5.3 Graph Efficiency V/s R Load

The proposed converter is also modelled with a PV array as a microsource and the output of the converter is connected to a

VSI (Voltage Sourse Inverter) and the simulation is carried out with the circuit. It is found that the inverter output is a sine wave with an output voltage of 400V. The Simulation model is shown in Fig. 5.4.

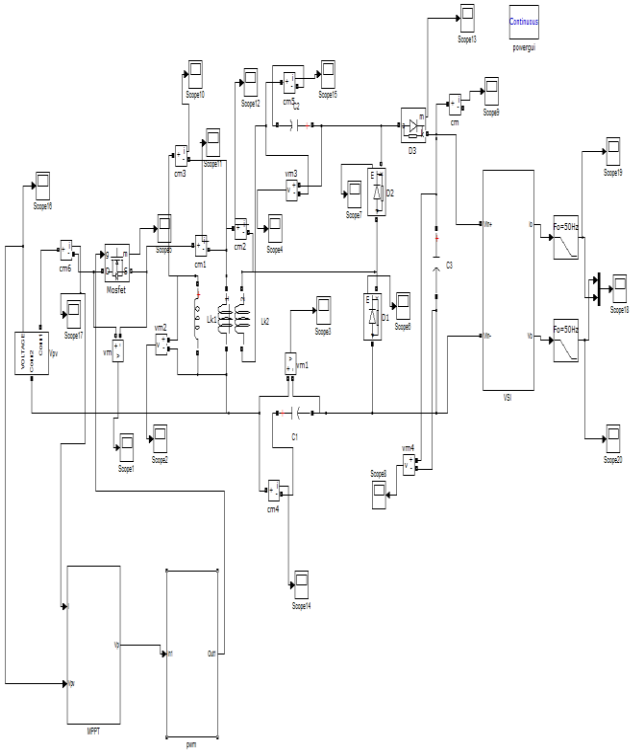

Fig: 5.4 Proposed converter with PV array connected as microsource.

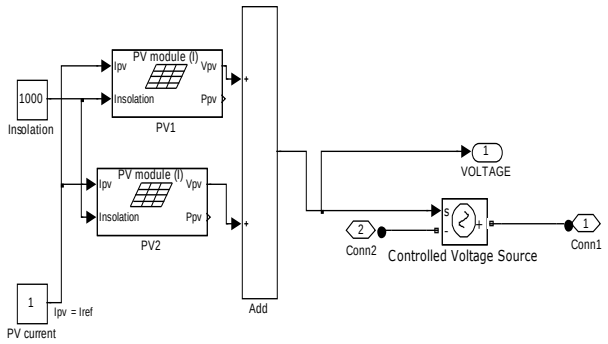

Fig: 5.5 Sub Circuit of the proposed converter showing PV array.

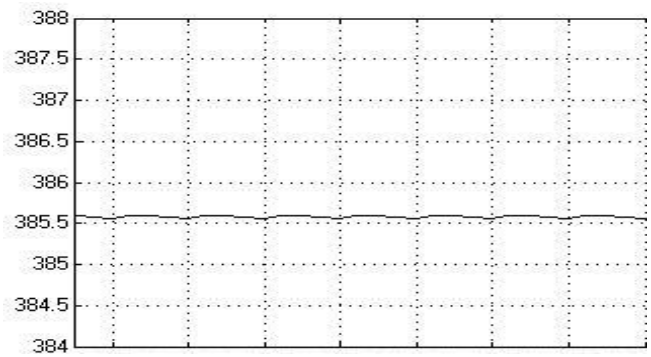

Fig: 5.6 Propose DC-Dc Converter Output Waveforms of Voltage.

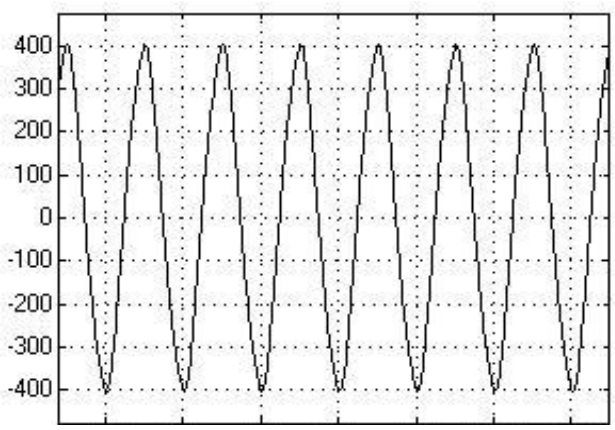

Fig: 5.7 Inverter Output Waveforms of Voltage.

VI. CONCLUSIONS

Since the energy of the coupled inductor's leakage inductor has been recycled, the voltage stress across the active switch S1 is constrained, which means low ON-state resistance R_{DS} (ON) can be selected. Thus, improvements to the efficiency of the proposed converter have been achieved. The switching signal action is performed well by the floating switch during system operation. From the simulation modeled converter, the turns ratio n = 5 and the duty ratio D is 55%; thus, without extreme duty ratios and turns ratios, the proposed converter achieves high step-up voltage gain, of up to 10 times the level of input voltage. The simulation results show that the maximum efficiency of 93%.

REFERENCES

[1] K. B. Park, G.W.Moon, and M. J. Youn, "Non isolated high step-up boost converter integrated with sepic converter," vol. 25, no. 9, pp. 2266–2275, Sep. 2010.

[2] T. Umeno, K. Takahashi, F. Ueno, T. Inoue, and I. Oota, "A new approach to low ripple- noise switching converters on the basis of switched- capacitor converters," in Proc. IEEE Int. Symp. Circuits Syst., Jun. 1991, pp. 1077– 1080.

[3] B. Axelrod, Y. Berkovich, and A. Ioinovici, "Transformer less dc–dc converters with a very high dc line-to-load voltage ratio," in Proc. IEEE Int. Symp. Circuits Syst. (ISCAS), 2003, vol. 3, pp. 435–438.

[4] Q. Zhao and F. C. Lee, "High-efficiency, high step-up dc–dc converters," IEEE Trans. Power Electron., vol. 18, no. 1, pp. 65–73, Jan. 2003.

[5] B. Axelrod, Y. Berkovich, and A. Ioinovici, "Switched-capacitor/ switched-inductor structures for getting transformer less hybrid dc–dc PWM converters," IEEE Trans. Circuits Syst. I, Reg. Papers, vol. 55, no. 2, pp. 687–696, Mar. 2008.

[6] L. S. Yang and T. J. Liang, "Analysis and implementation of a novel bidirectional dc–dc converter," IEEE Trans. Ind. Electron., vol. 59, no. 1, pp. 422–434, Jan. 2012.

[7] W. Li and X. He, "Review of non-isolated high-step-up dc/dc converters in photovoltaic grid-connected applications," IEEE Trans. Ind. Electron., vol. 58, no. 4, pp. 1239–1250, Apr. 2011.

[8] S. H. Park, S. R. Park, J. S. Yu, Y. C. Jung, and C. Y. Won, "Analysis and design of a soft-switching boost converter with an HI-Bridge auxiliary resonant circuit," IEEE Trans. Power Electron, vol. 25, no. 8, pp. 2142– 2149, Aug. 2010.

